

## Results from the Relativistic Heavy Ion Collider

BEDANGADAS MOHANTY\*

Variable Energy Cyclotron Centre, 1/AF, Bidhan Nagar, Kolkata-700064, India

(Received 28 February 2006; Accepted on 5 September 2006)

The Relativistic Heavy Ion Collider (RHIC) at Brookhaven National Laboratory is the only dedicated machine for research in the field of high energy heavy-ion collisions. Four experiments namely BRAHMS, PHOBOS, PHENIX and STAR, use this facility to study the properties of matter formed when two heavy ions collide at very high center of mass energies. A lot of interesting data have come out of RHIC experiments, which suggest formation of a hot and dense matter in the heavy ion collisions, which is one of the pre-requisite of quark gluon plasma (QGP) formation. We discuss the recent important results from the four experiments. Results based on identified particle production and particle ratio, strange particle enhancement, suppression of hadron production at high transverse momentum relative to nucleon-nucleon collisions, azimuthal flow, direct photon and  $J/\psi$  production are presented. We also discuss the first results from the photon multiplicity detector, the Indian group contribution to RHIC.

**Key Words:** PACS numbers

### Introduction

There has always been a considerable interest in knowing about the fate of nuclear matter when subjected to extremes of density and temperature. Particularly intriguing was the suggestion that new phases of nuclear matter could be associated with a corresponding change in the structure of the vacuum [1]. This vacuum structure is modified at high temperatures and/or densities, suggesting that quarks and gluons under such conditions would be deconfined [2]. In Table 1 we mention the difference in properties of vacuum and a hot and dense matter as predicted by Quantum Chromodynamics (QCD), the fundamental theory for strong interactions. In other words, when the energy density exceeds some typical hadronic value ( $>1 \text{ GeV}/\text{fm}^3$ ), matter no longer consists of separate hadrons (protons, neutrons, etc.), but as their fundamental constituents, quarks and gluons. Because of the apparent analogy with similar phenomena in atomic physics we may call this phase of matter the QCD (or quark-gluon) plasma. Lattice QCD [3] predicts a phase transformation to a quark-gluon plasma (QGP) at a temperature of approximately  $175 \text{ MeV} \sim 10^{12} \text{ K}$ . The Lattice QCD calculations showing how the potential between the partons vanishes for high temperature leading to deconfined state is shown in Fig. 1 One of the primary goals of the relativistic heavy ion collider (RHIC) is the experimental study of the QCD phase transition by colliding heavy ions (Au+Au and Cu+Cu) at various high energies (19.6 GeV to 200 GeV).

In this manuscript we shall discuss the most recent results from RHIC [5-8], in terms of the bulk properties

of the hadron production (transverse momentum

**Table 1: Interesting features for QCD of vacuum and QCD of hot and dense matter**

QCD in Vacuum	QCD in hot and dense matter
linear increase in potential with distance from color charges	screening of color charges
strong attractive force	potential vanishes at large distance scales
spontaneous breaking of chiral symmetry	restoration of chiral symmetry
confinement of quarks to hadrons	deconfinement

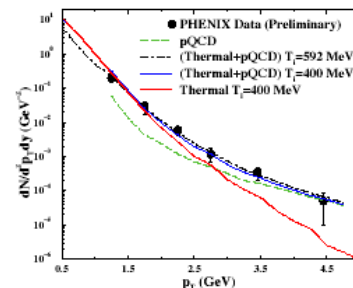


**Fig. 1:** The color averaged heavy quark free energy at various temperatures in the low temperature phase of three flavour QCD. Figure taken from Ref.[4]

spectra, particle ratios) and the penetrating probes which includes high transverse momentum particle production,  $J/\psi$  production and thermal radiation. We will also discuss the Indian effort in this field, through the design, fabrication, commissioning and successful data taking of our photon multiplicity detector (PMD) in STAR experiment at RHIC.

### Bulk Properties

\* Email: bmohanty@veccal.ernet.in

The multiplicities, yields, momentum spectra and correlations of hadrons emerging from heavy-ion collisions, especially in the soft sector comprising particles at transverse momenta,  $p_T < 1.5$  GeV/c, reflect the properties of the bulk of the matter produced in the collision. Here we only discuss about  $P_T$  spectra and particle ratios.

The measured hadron spectra reflect the properties of the bulk of the matter at kinetic freeze-out, after elastic collisions among the hadrons have ceased. Somewhat more direct information on an earlier stage can be deduced from the integrated yields of the different hadron species, which change only via inelastic collisions. The point where these inelastic collisions cease is referred to as chemical freeze-out and usually takes place before kinetic freeze-out. The transverse momentum distributions of the different particles reflect a random and a collective component. The random component can be identified with the temperature of the system at kinetic freeze-out. The collective component which arises from the matter density gradient from the center to the boundary of the fireball created in high-energy nuclear collisions is called as collective flow. This collective flow is sensitive to the Equation of State of the expanding matter.

### Transverse Momentum Spectra

The characteristics of the system at kinetic freeze-out can be explored by analysis of the transverse momentum distributions for various hadron species, some of which are shown in Fig. 2. In order to characterize the transverse motion, hydrodynamics-motivated fits [9] have been made to the measured spectra, permitting extraction of model parameters characterizing the random (generally interpreted as a kinetic freeze-out temperature  $T_{fo}$ ) and collective (radial flow velocity ( $\beta_T$ )) aspects. Results for these parameters are shown for different centrality bins and different hadron species in Fig. 3.

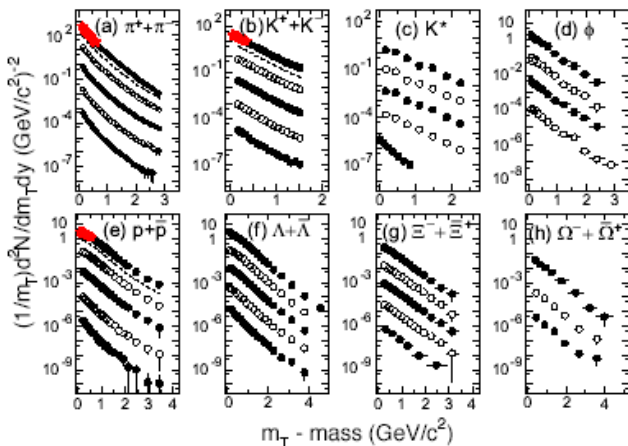


**Fig. 2:** Mid-rapidity hadron spectra from  $\sqrt{SNN} = 200$  GeV Au+Au collisions. The spectra are displayed for decreasing

centrality from the top to downwards within each frame, with appropriate scaling factors applied for clarity of presentation. For  $K^+$  only, the lowest spectrum shown is for 200 GeV p+p collisions. The dashed curves in frames (a), (b) and (e) represent spectra from minimum-bias collisions. The invariant spectra are plotted as a function of  $m_T - \text{mass} \sqrt{p_T^2/c^2 + \text{mass}^2} - \text{mass}$

As the collisions become more and more central, the bulk of the system, dominated by the yields of  $\pi$ ,  $K$ ,  $p$ , appears from Fig. 3 to have lower kinetic freeze-out temperature and to develop stronger collective flow. On the other hand, even for the most central collisions, the spectra for multi-strange particles  $\phi$  and  $\Omega$  appear to reflect a higher freeze-out temperature.

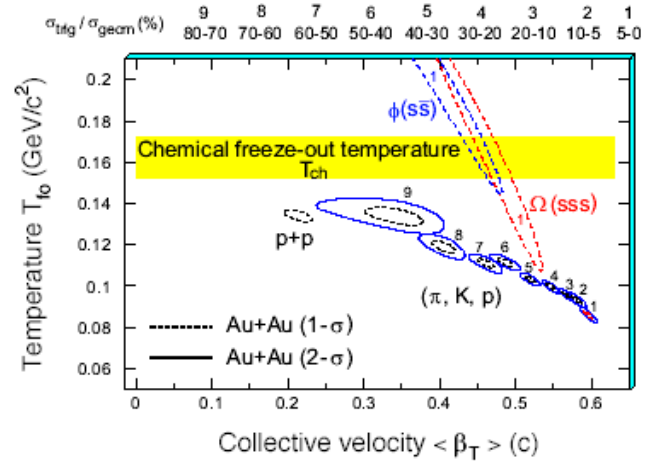


**Fig. 3:** The  $\chi^2$  contours, extracted from thermal + radial flow fits (without allowance for resonance feed-down), for produced hadrons  $\pi$ ,  $K$  and  $p$  and multi-strange hadrons  $\phi$  and  $\Omega$ . On the top of the plot, the numerical labels indicate the centrality selection. For  $\pi$ ,  $K$  and  $p$ , 9 centrality bins (from top 5% to 70-80%) were used for  $\sqrt{SNN} = 200$  GeV Au+Au collisions [7]. The results from p+p collisions are also shown. For  $\phi$  and  $\Omega$ , only the most central results are presented. Dashed and solid lines are the 1- $\sigma$  and 2- $\sigma$  contours, respectively.

### Particle Ratios

Figure 4 compares STAR measurements of integrated hadron yield ratios for central Au+Au collisions to statistical model fits. In comparison to results from p+p collisions at similar energies, the relative yield of multi-strange baryons  $\Xi$  and  $\Omega$  is considerably enhanced in RHIC Au+Au collisions [7]. The measured ratios are used to constrain the values of system temperature and baryon chemical potential at chemical freeze-out, under the statistical model assumption that the system is in thermal and chemical equilibrium at that stage. The excellent fit obtained to the ratios in the figure, including stable and long-lived hadrons through multi-strange baryons, is consistent with the light flavors,  $u$ ,  $d$ , and  $s$ , having reached chemical equilibrium (for central and near-central collisions only) at  $T_{ch} = 163 \pm 5$  MeV<sup>7</sup>. The deviations

of the short-lived resonance yields, such as those for  $\Lambda^*$  and  $K^*$  collected near the right side of Fig. 4, from the statistical model fits, presumably result from hadronic re-scattering after the chemical freeze-out and needs to be further understood.

The saturation of the strange sector yields, attained for the first time in near-central RHIC collisions, is particularly significant. The saturation is indicated quantitatively by the value obtained for the non-equilibrium parameter  $\gamma_s$  for the strange sector for central collisions. The temperature deduced from the fits is essentially equal to the critical value for a QGP-to-hadron-gas transition predicted by Lattice QCD [3], but is also close to the Hagedorn limit for a hadron resonance gas, predicted without any consideration of quark and gluon degrees of freedom [10]. If thermalization is indeed achieved by the bulk matter prior to chemical freeze-out, then the deduced value of  $T_{ch}$  represents a lower limit on that thermalization temperature.

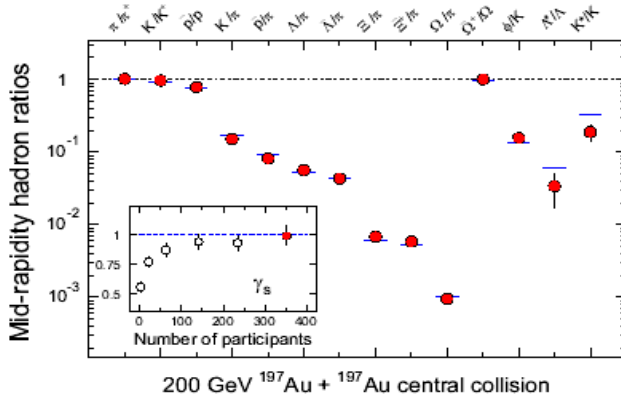


**Fig. 4:** Ratios of  $p_T$ -integrated mid-rapidity yields for different hadron species measured in STAR, for central Au+Au collisions at  $\sqrt{s_{NN}} = 200$  GeV. The horizontal bars represent statistical model fits to the measured yield ratios for stable and long-lived hadrons. The fit parameters are  $T_{ch} = 163 \pm 4$  MeV,  $\mu_B = 24 \pm 4$  MeV,  $\gamma_s = 0.99 \pm 0.07$ . The variation of  $\gamma_s$  with centrality is shown in the inset, including the value (leftmost point) from fits to yield ratios measured by STAR, for 200 GeV  $p+p$  collisions.

### Penetrating Probes

We shall discuss two broad classes of penetrating probes: (a) Hard probes created at the very early stage of the collision which propagate through, and could be modified by, the medium. These are high- $p_T$  particles coming from the fragmentation of jets and hidden charm ( $J/\psi$  production) production, (b) Electromagnetic probes (photons or di-leptons) which are created by the medium. Due to their large mean free path these probes can leave the medium without final-state interaction thus carrying direct information about the medium's conditions and properties.

#### A. High $p_T$ Particle Production

The most exciting results to date at RHIC are the discovery of high- $p_T$  suppression of mesons in nucleus-

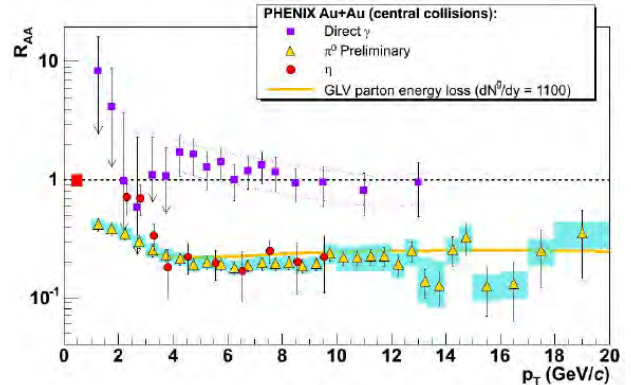
nucleus collisions compared to binary collision scaled  $p+p$  collision data. This has been interpreted in terms of energy loss of quarks in a high-density medium. The other interesting aspect seen is the non-suppression of baryons or equivalently, the anomalously high  $p/\pi$  ratio.

The results on high- $p_T$  suppression are usually presented in terms of the nuclear modification factor  $R_{AA}$ , defined as:

$$R_{AA} = \frac{dN_{AA}/d\eta d^2p_T}{T_{AB} d\sigma_{NN}/d\eta d^2p_T} \quad \dots(1)$$

where the overlap integral  $T_{AB} = N_{binary}/\sigma_{inelastic}^{pp}$

In figure 5 we show PHENIX preliminary data for the  $R_{AA}$  of  $\pi^0$  in central Au+Au collisions in the  $p_T$  range up to 20 GeV/c [8]. The suppression is very strong, and it is flat at  $R_{AA} \simeq 0.2$  up to 20 GeV/c. There is no hint that it returns to unity. The figure also shows that the suppression of  $\pi^0$ 's and  $\eta$ 's is very similar, which supports the conclusion that the suppression occurs at the parton level, not the hadron level. This strong suppression of mesons is in contrast to the behavior of direct photons, also shown in the figure. The direct photons follow binary scaling (i.e.  $R_{AA} \simeq 1$ ). This is strong evidence that the suppression is not an initial state effect, but a final state effect caused by the high density medium created in the collision. The curve



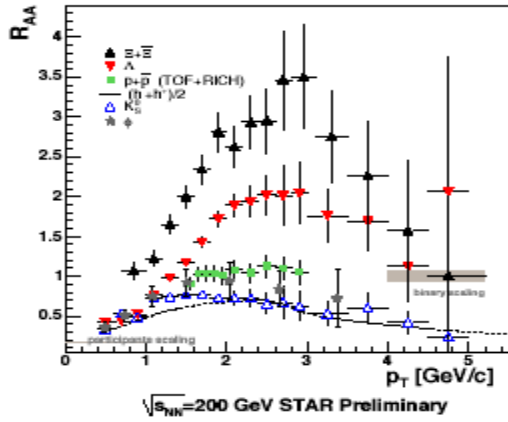


**Fig. 5:** Nuclear modification factor,  $R_{AA}$  of  $\pi^\circ$  (triangles),  $\eta$  (circles), and direct photon (squares).  $R_{AA}$  at  $\sqrt{s_{NN}} = 200$  GeV with respect to  $p_T$ .  $R_{CP}$  ratio is calculated for 0-5% over 40-60% central AuAu collisions and  $R_{AA}$  is for 0-5% central AuAu collisions over normalized min-bias pp collisions for the given energies.

the plot shows a theoretical prediction [11] using the GLV parton energy loss model. The model assumes an initial parton density  $dN/dy = 1100$ , which corresponds to an energy density of approximately  $15 \text{ GeV}/\text{fm}^3$ . The data show that the suppression is somewhat stronger than the prediction, suggesting that the matter density may be even higher than these estimates.

The measurement of  $R_{AA}$  (0-5% Central AuAu/Scaled Minbias pp) from STAR experiment with respect to  $P_T$  is shown in Fig. 5. While the measurements for mesons ( $h^+ + h^-$ ,  $K_S^0$ ,  $\phi$ )  $R_{AA}$  are suppressed,  $R_{AA}$  of strange baryons shows significant differences. Strange baryons do not show any suppression. Instead there is an enhancement and ordering with strangeness content: the higher the strangeness content, the higher the  $R_{AA}$  measurement in the intermediate  $P_T$  region.

The baryon and meson differences observed at intermediate  $P_T$  region is explained reasonably well (at least the trends) by assuming that hadron formation at moderate  $P_T$  proceeds via two competing mechanisms: the coalescence of  $n_q$  constituent quarks at transverse momenta  $\sim p_T/n_q$ , drawn from a thermal (exponential) spectrum, plus more traditional fragmentation of hard-scattered partons giving rise to a power-law component of the spectrum. This comparison to STAR data is shown in the Fig. 6.

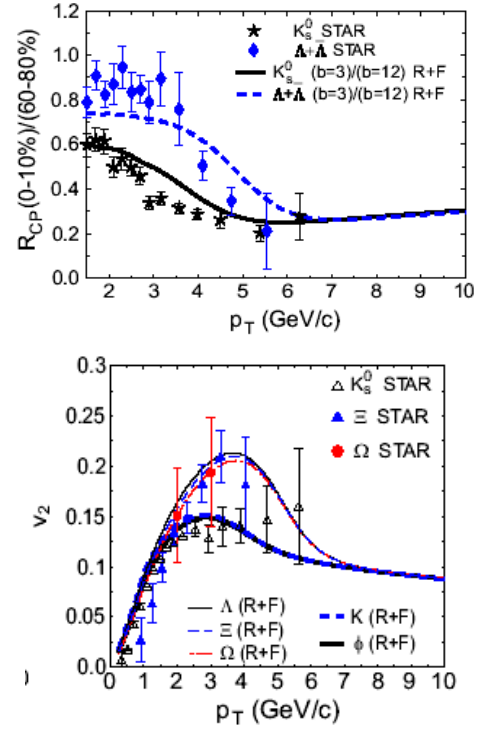


**Fig. 6:** Comparisons of calculations in the Duke quark recombination model with STAR, measurements of (a)  $B_{CP}$  and (b)  $v_2$  for strange mesons and baryons. "R+F" denotes the sum of recombination and fragmentation contributions. Comparison of the solid and broken curves in (b) reveals a weak mass-dependence in the calculations, superimposed on the predominant meson-baryon differences. The figures are taken from Ref. [12], and they include preliminary STAR, data for multi-strange baryons

### $J/\psi$ Production

The suppression in production of  $J/\psi$ s created in nuclear collisions when the system size and the centrality of the collision increase [8] has been predicted to be a signature for the formation of quark gluon plasma. The PHENIX collaboration has reported the preliminary results on the nuclear modification factor for  $J/\psi$ s in Au+Au, Cu+Cu and d+Au collisions at  $\sqrt{s_{NN}} = 200$  GeV. The experiment measures  $J/\psi \rightarrow e^+e^-$  decay at mid rapidity ( $|\eta| < 0.35$ ) and  $J/\psi \rightarrow \mu^+\mu^-$  decay at forward rapidity ( $|\eta| \in [1.2, 2.2]$ ).

Figure 7 represents the  $J/\psi$  nuclear modification factor as a function of the number of participating nucleons. A suppression of about a factor 3 is observed for the most central collisions.

### Thermal Radiation

Electromagnetic probes have been proposed to be one of the most promising tools to characterize the initial state of the collisions. Because of the very nature of their interactions photons and dileptons suffer minimum re-scattering and therefore, can be used as an efficient tool to extract the initial temperature of the system. The PHENIX collaboration has analyzed the

data by using a novel technique and reported excess direct photons over the next to leading order perturbative QCD (NLO pQCD) processes for Au + Au collisions at  $\sqrt{s} = 200A$  GeV. This is shown in Fig. 8.

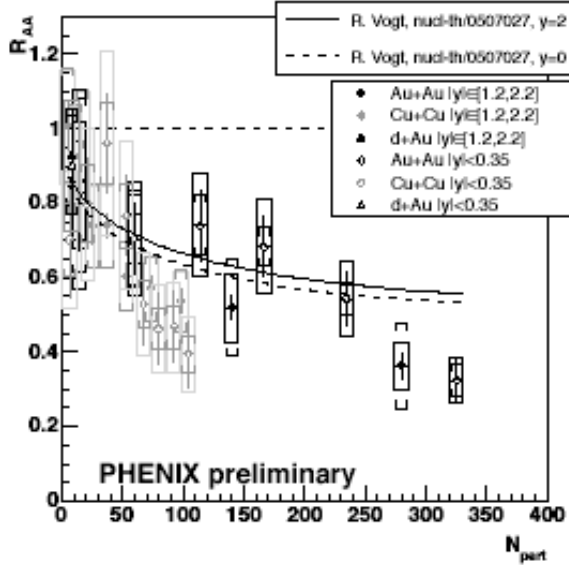


Fig. 7:  $J/\psi$  nuclear modification factor as a function of the number of participant, compared to  $R_{AA}$ . Vogt predictions for the normal nuclear absorption. Vertical bars are statistical errors, brackets are point to point systematics and boxes are global systematics.

The experimental data has been compared to hydrodynamical calculations [13]. The data can be reproduced by assuming a deconfined state of quarks and

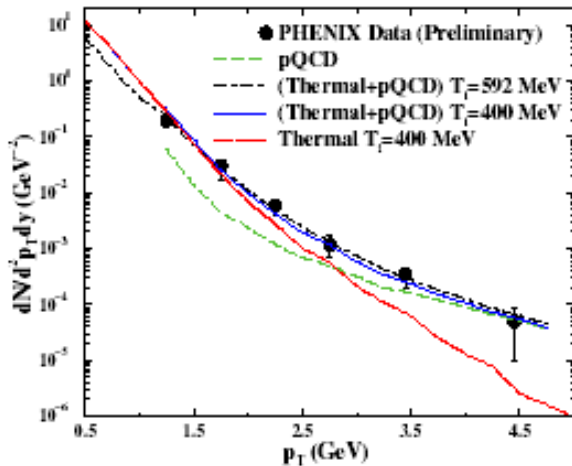


Fig. 8: Direct photon spectra at RHIC energies measured by PHENIX Collaboration. Dashed line indicates hard photons from NLO pQCD calculations. Solid (dot-dashed) line depicts the total (pQCD + thermal) photon yield obtained from QGP initial state with  $T_i = 400$  MeV and  $n = 0.2/m/c$  ( $T_i = 592$  MeV  $n = 0.15$  fm/c). In medium effects on hadrons are included (ignored) in the results shown by solid (dot-dashed) line.

gluons with initial temperature  $\sim 400$  MeV and thermalization time scale  $\sim 0.2$  fm/c. The extracted

average temperature ( $T_{av}$ ) from photon spectra is found to be  $\sim 265$  MeV for the  $p_T$  range 1.25 to 2.25 GeV where thermal contributions dominate. When the flow effect is subtracted out from  $T_{av}$ , the 'true' average temperature is found to be 215 MeV. This indicates that the initial temperature must be more than 215 MeV because the thermal photon spectra is a superposition of emission rates for all the temperatures from initial to freeze-out. So the temperature of the system formed after the collisions is higher than the transition temperature for deconfinement predicted by lattice QCD.

At higher  $p_T$ , the parton cascade calculations of single photon yield including the Landau-Pomeranchuk-Midgal effect [14] has been shown to be in good agreement with the PHENIX data taken at the Relativistic Heavy-Ion Collider [8].

### Indian Contribution in STAR Experiment at RHIC

The main Indian group contribution to RHIC is in the form of a photon multiplicity detector (PMD). There is also an active participation of Indian group in the PHENIX experiment at RHIC. In this section we shall only focus on the results from the PMD at RHIC. The STAR PMD [15] consists of a set of supermodules arranged in two vertical halves so that each half moves independently around the beam pipe. The supermodules are of various shapes but all are made up of rhombus unit modules having 24x24 cells. The number of unit modules in the supermodules vary from 4 to 9. There are two planes of the sensitive detectors, one in front of the 3 radiation length lead converter (acting as charged particle veto) and one behind the converter which registers preshower signals. There are 12 supermodules in each plane of the detector. Each unit module consists of an array of hexagonal cells made up of copper and filled with a gas mixture of Argon and Carbon dioxide in the ratio of 70:30. Each plane of PMD consists of a total of 41,472 cells. Each cell acts as a gas proportional counter, with the copper cell acting as a cathode. There is a thin gold plated tungsten wire passing through the center which acts as an anode wire. The cathode is slightly extended to have a higher charged particle detection efficiency and is given a negative high voltage of about 1400 V. The ionization signal produced when a charged particles passes through the gas is readout from the anode. The cell design and the operating conditions (gas mixture and high voltage) of the detector was arrived at after detailed simulations and tests with prototype detectors. These informations can be found in Ref. [15,16].

The principle of photon detection in PMD is as follows. A photon traversing the converter produces an electromagnetic shower in the preshower plane, leading to a larger signal spread over several cells as compared to a charged particle, which is essentially confined to one cell. The number of cells hit in the preshower plane and the energy deposited are used for

discriminating photons and hadrons falling on the detector.

The signal processing for STAR PMD is done using GASSIPLEX chips, which has 16 channels of preamplifier and shaper and provides analog multiplexed output. One front-end electronics (FEE)-Board has 4 chips and is connected to a group of 64 cells in a 8x8 matrix on the detector. The digitization and readout of the analog multiplexed signals is done using C-RAMS modules. The track and hold flag is generated using a pre-trigger signal based on beam-beam counter in STAR because the actual Level 0 signal arrives rather late. Each block of C-RAMS handles signals from a chain of 27 FEE boards, i.e., for 1728 cells. There are in all 48 chains read out using 24 C-RAMS modules.

The detector is mounted in the STAR experiment at 540cm from the center of the TPC and nominally covers the pseudorapidity region 2.3-3.8 with full azimuthal acceptance. Particle production models at RHIC suggests about 10-11% of the total produced photons fall within the acceptance of PMD. The photons produced in the collisions is dominated by photons from the decay of  $\pi^0$ . Model calculations suggest that about 93-96% of the photons are from the inclusive  $\pi^0$  decays.

Fully instrumented preshower plane of the STAR PMD is shown in Fig. 9 in the data taking mode when the two halves are touching each other.

First results on photon distribution in the forward region at 62.4 GeV energy recently became available with the PMD in the STAR experiment [17]. In Fig. 10

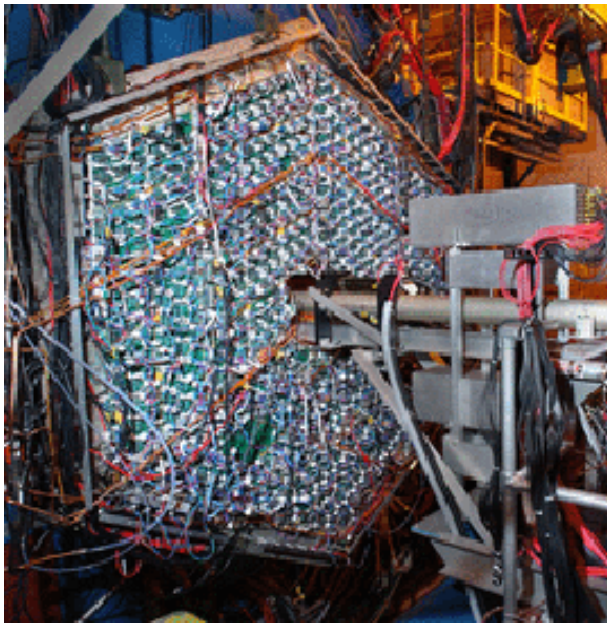


**Fig. 9:** View of the preshower plane of STAR, PMD from the RHIC tunnel side

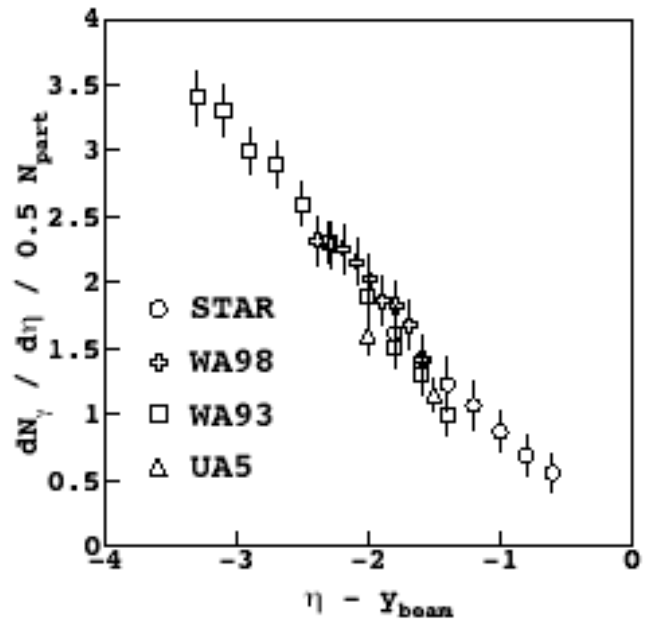


**Fig. 10:** Limiting fragmentation in the photon production

we have plotted the photon pseudorapidity distribution per participant nucleon in Au+Au collisions at 62.4A GeV as a function of  $\eta - y_{beam}$  for central collisions. Also superposed are the data from the WA98 experiment for the Pb+Pb collisions at 17.A GeV c.m. energy, from the WA93 experiment for S+Au collisions at 20.A GeV c.m. energy and from the UA5 experiment for  $pp$  collisions at 546 GeV. The data at SPS and at RHIC are found to be consistent with each other, suggesting that photon production follows the limiting fragmentation hypothesis. It is further found that the data are consistent with impact parameter and energy independent behaviour.

### Summary

In summary, there is strong experimental evidence that heavy-ion collisions at RHIC produce a state of matter characterized by very high energy densities, density of unscreened color charges ten times that of a nucleon, large cross sections for the interaction between strongly interacting particles, strong collective flow, and early thermalization. Measurements indicate that this matter modifies jet fragmentation and has opacity that is too large to be explained by any known hadronic processes. This state of matter is not describable in terms of ordinary color-neutral hadrons, because there is no known self-consistent theory of matter composed of ordinary hadrons at the measured densities. The most economical description is in terms of the underlying quark and gluon degrees of freedom. Models taking this approach have scored impressive successes in explaining many, but not all, of the striking features measured to date. Determining whether the quarks and gluons in this matter reach thermal equilibrium with one another before they become confined within hadrons, and eventually

whether chiral symmetry is restored, are two among many profound questions one may ask as we move from the initial discovery phase of dense partonic matter to the next phase of probing the properties of the matter created at RHIC. Indian photon multiplicity detector at RHIC has successfully taken data. The first results from this detector has contributed to significant understanding of the particle production mechanism at RHIC [17].

## References

1. T D Lee, *Trans N Y Acad Sci Ser* **2v.40** (1980) 0111.
2. J C Collins, M J Perry, *Phys Rev Lett* **34** (1975) 1353.
3. F Karsch, *Lecture Notes in Physics* **583** (2002) 209.
4. F Karsch and E Laermann, hep-lat/0305025.
5. BRAHMS Collaboration, I Arsene et al, *Nucl Phys A* **757** (2005) 1.
6. PHOBOS Collaboration, B B Back et al, *Nucl Phys A* **757** (2005) 28.
7. STAR, Collaboration, J Adams *et al*, *Nucl Phys A* **757** (2005) 102.
8. PHENIX Collaboration, K Adcox *et al*, *Nucl Phys A* **757** (2005) 184.
9. E Schnedermann, J Sollfrank and U Heinz, *Phys Rev C* **48** (1993) 2462.
10. R Hagedorn, *Nuovo Cim Suppl.* **3** (1965) 147.
11. I Vitev and M Gyulassy, *Phys Rev Lett* **89** (2002) 252301.
12. B Miiller, nucl-th/0404015; R J Fries, B Muller, C Nonaka, and S A Bass, *Phys Rev Lett* **90** (2003) 202303.
13. Jan-e Alam, Jajati K Nayak, Pradip Roy, Abhee K Dutt-Mazumder and Bikash Sinha, nucl-th/0508043.
14. Thorsten Renk, Steffen A Bass and Dinesh K Srivastava, nucl-th/0505059.
15. Aggarwal MM et al, *Nucl Instr Meth* **A499** (2003) 751.
16. Aggarwal MM et al, *Nucl Instr Meth* **A488** (2002) 131.
17. Adams J et al, STAR, Collaboration, *Phys Rev Lett* **95** (2005) 062301.

